Received 11 July 2023, accepted 31 July 2023, date of publication 7 August 2023, date of current version 17 August 2023.

Digital Object Identifier 10.1109/ACCESS.2023.3302525

RESEARCH ARTICLE

Robust Trajectory Tracking of Delta Parallel Robot Using Fractional-Order Sliding Mode Control

BEHNOUSH ALIZADEH, AHMAD HAJIPOUR, HAMIDREZA TAVAKOLI, AND ABBAS NASRABADI
Faculty of Electrical and Computer Engineering, Hakim Sabzevari University, Sabzevar 9617976487, Iran
Corresponding author: Ahmad Hajipour (a.hajipour@hsu.ac.ir)

ABSTRACT In this study, a Fractional-Order Sliding Mode Control scheme is proposed for trajectory tracking control of Delta parallel robot. The proposed controller is compared with both integer-order Proportional-Derivative controller and integer-order Sliding Mode Controller with Computed Torque Control method. The forward kinematics, inverse kinematics and dynamic of Delta parallel robot are described. A Solidworks/Matlab/SimScape/Multibody model of Delta parallel robot is generated and used for dynamic parameter estimation and validation of the proposed method. Particle Swarm Optimization algorithm is utilized for dynamic parameter estimation of Delta parallel robot. The validation of the proposed method is evaluated for three different trajectories. External disturbances, noise and also various payloads are considered in testing robustness of control techniques. The results of the robustness tests confirm higher performance of FOSMC than two other control schemes.

INDEX TERMS Delta parallel robot, fractional-order sliding mode control, trajectory tracking, parameter estimation.

I. INTRODUCTION

In modern industry, mass production requires high speed and high precision robots. For this reason, robotics and its relevant topics have gained significant attention among researchers. Due to their relatively lower speed and higher error, serial robots are being replaced with parallel robots.

Delta parallel robots with three or four Degrees of Freedom (DOF) are of the most important parallel robots which are being used widely in food industry, haptic devices, pharmaceutical, cosmetics and etc. Over the past two decades, a lot of research have been conducted on Delta parallel robot such as dynamic model, workspace, trajectory tracking control and etc. [1], [2], [3], [4], [5], [6], [7], [8].

One of the important issues for parallel robot is to keep it on its path, preventing collision with obstacles, while moving it along shortest path from its starting point to its target. In most applications, the robot should quickly move from one position to another or track repeatedly a desired trajectory in 3D space with high accuracy. Due to model uncertainties, time-varying nonlinear dynamic effects, noise, external disturbances and payload variations, achieving high performance in trajectory tracking is difficult. In order to achieve good tracking and high precision in position control, it is necessary to use nonlinear controllers to cope with mentioned problems. Recently, various control methods such as computed torque via Proportional-Integral-Derivative (PID) controller [9], Sliding Mode Controller (SMC), H_∞ or Quantitative Feedback Theory (QFT) [10], [11], [12] have been applied to Delta parallel robot.

In [13], H_∞ has been used for external disturbances and uncertainties in a system. The performance of H_∞ has been compared with PID controller in [10]. For designing PID controllers, dynamic model of Delta robot should be linearized at an operational point. Since the system has several operating points, the controller may not perform well for other points. The design and implementation of H_∞ strategy is too complicated. The computed torque technique

The associate editor coordinating the review of this manuscript and approving it for publication was Laxmisha Rai.

via PID controller is low cost and simple to implement, but it cannot achieve a good performance in presence of uncertainties and disturbances.

Sliding Mode Control (SMC) is a strong robust control scheme for nonlinear systems with uncertainties, unmodeled dynamics and disturbances which has been widely used in literature [14], [15], [16], [17]. In order to improve the dynamic performance of the system, it is necessary to choose a special type of SMC technique while its parameters should also be precisely determined. Recently, a number of SMC techniques for reducing the effect of chattering phenomenon during control process have been proposed in the literature [16], [18], [19], [20], [21], [22].

Fractional-Order Sliding Mode Control (FOSMC) is a robust control technique that is based on fractional computations, providing more flexibility compared to traditional integer-order control methods. FOSMC is particularly effective for achieving high-precision control of nonlinear systems, with its robustness, small chattering, fast reaching ability, and high steady-state accuracy. [23], [24], [25], [26], [27], [28], [29], [30], [31].

On the other hand, accurate determination of dynamic parameters of a robot plays important role in designing model-based controllers. Nonlinear load besides their complex structure make it difficult to determine precisely dynamic parameters of parallel robots. Estimation from measured experimental values is the only effective method to determine accurate parameters of a dynamic model. A number of theoretical and experimental studies on parameter estimation have been introduced in the literature [32]. Recently, many evolutionary algorithms such as genetic algorithm [33], Particle Swarm Optimization (PSO) [34], [35], [36], [37], cuckoo search [38] and etc. have been reported for modeling, parameter estimation and tuning of controller parameters in the literature.

According to the above mentions, contribution of this paper can be summarized in the following points:

- A methodology for parametric identification of the dynamic model of a Delta parallel robot is presented. The dynamic behavior of Delta robot is simulated by Solidwork - Matlab co-simulation model. The parameters of the robot dynamic model are estimated by PSO algorithm.
- Using advantages of fractional calculations and sliding mode control, FOSMC is proposed and implemented for trajectory tracking in 3-DOF Delta parallel robot. FOSMC is used to improve precision, robustness, fast finite-time convergence and to reduce chattering during desired motion.
- To illustrate performance of the proposed controller, the results of its implementation are compared with PD and SMC controllers using robustness analysis i.e. evaluation with applying external disturbance, evaluation with applying critical payload and evaluation in presence of noise.

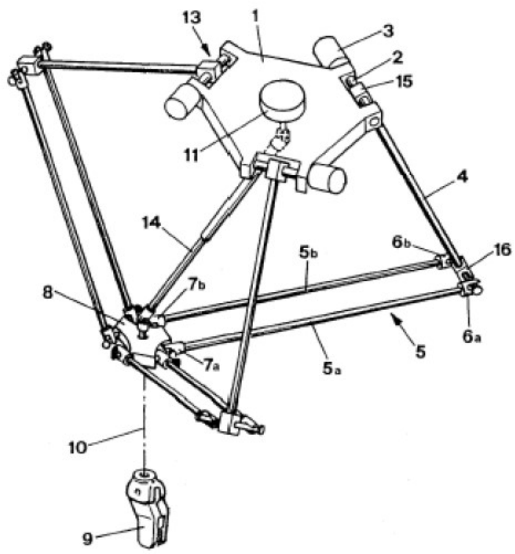

FIGURE 1. Schematic of delta parallel robot.

This paper is organized as follows: In section II, forward and inverse kinematics and dynamic model of Delta robot are presented. Estimation methodology of dynamic model parameters with PSO algorithm is described in section III. Tracking control strategies and comparing their performances are presented in sections IV and V, respectively. In section VI, results of the robustness test of proposed controllers are presented. Conclusions are given in section VII.

II. MECHANIC OF DELTA PARALLEL ROBOT

In this section, forward and inverse kinematics, dynamical and SimScape multibody models are described for Delta parallel robot.

Delta robot, invented by Reymond Clavel [39], has three revolute actuators providing 3 degrees of freedom of displacement in x, y and z coordinates. This is the most successful commercial parallel robot and it is commonly used for high speed and high precision tasks. The original design from Clavel U.S. patent [40] is shown in Fig. 1.

A prototype of Delta parallel robot which has been fabricated in mechatronics lab of Hakim Sabzevari University is shown in Fig. 2. This robotic system will be used to implement and validate advanced control algorithms.

Kinematics describes motion of systems without considering forces that cause them to move. Geometric structure of Delta parallel robot is shown in Fig. 3. As can be seen in the figure, origin of global coordinate system $\{X, Y, Z\}$ of Delta robot is located at the center of the fixed plate. Coordinate system $\{X_n, Y_n, Z_n\}$ for end effector is located at point n. The end effector is connected to fixed plate via three kinematic chains.

From Fig. 4, a and b are the upper and the lower arm lengths, respectively. The upper arms are mounted on three actuators that are located in the fixed plate with radius r_a

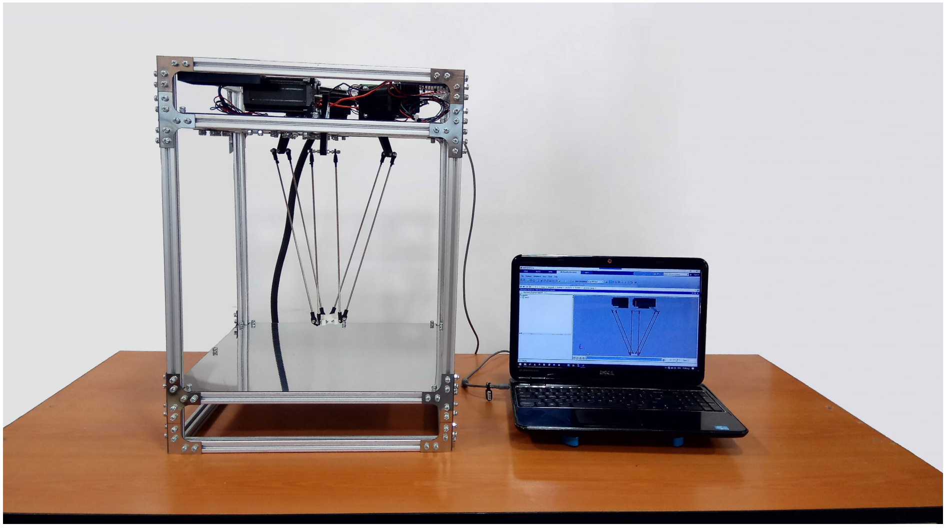

FIGURE 2. Delta parallel robot prototype fabricated in Hakim Sabzevari University.

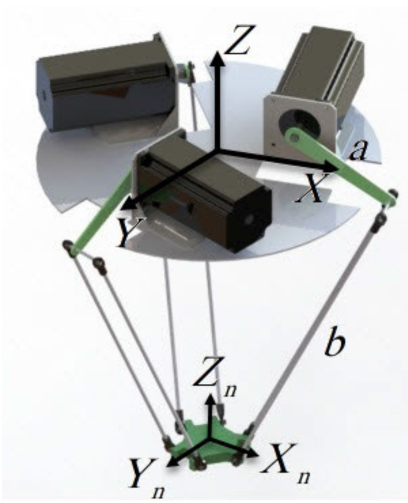

FIGURE 3. Geometric structure of delta parallel robot.

and angle $\phi_i = (0°, 120°, 240°)$. r_b denotes the radius of end effector.

A. INVERSE KINEMATICS OF DELTA ROBOT

The inverse kinematics determines joints position θ_i of Delta parallel robot with respect to spatial position of end effector in the global coordinate system $\{X, \ Y, \ Z\}$. The connection points of links a and b create restrictions. These restrictions are the shape of spheres with centers at points t_i and radius b in which $i = 1, 2, 3$. Mentioned spheres are described as follows:

$$(x - x_i)^2 + (y - y_i)^2 + (z - z_i)^2 = b^2 \tag{1}$$

The intersection of mentioned spheres and $x - z$ plane creates circles with centers at point u_i and radius a. The circles

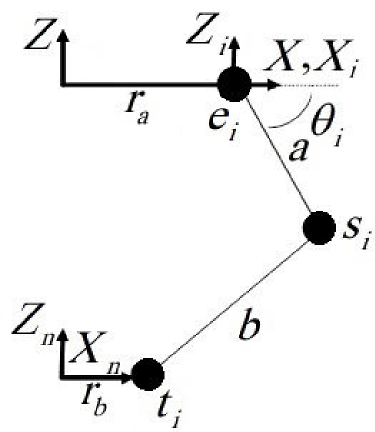

FIGURE 4. Arm of delta parallel robot.

equations are as follows:

$$(x - r_a)^2 + z^2 = a^2 \tag{2}$$

By combining and simplifying Eq. (1) and Eq. (2), joint space variables can be obtained as follows:

$$\theta_i = \sin^{-1}\left(\frac{z}{a}\right) \tag{3}$$

In Eq. (3), two solutions are obtained that only one of them could be accepted. To prevent singularity, following restriction is defined for all joint variables.

$$\begin{cases} \theta_i = \sin^{-1}\left(\frac{z}{a}\right); & x - r_a \geq 0, \\ \theta_i = \pi - \theta_i; & x - r_a < 0. \end{cases} \tag{4}$$

B. FORWARD KINEMATIC OF DELTA ROBOT

Forward kinematics determines position of end effector $\{X_n, Y_n, Z_n\}$ based on joint variables. Three spheres mentioned in Eq. (1) and three circles at the center point s_i with

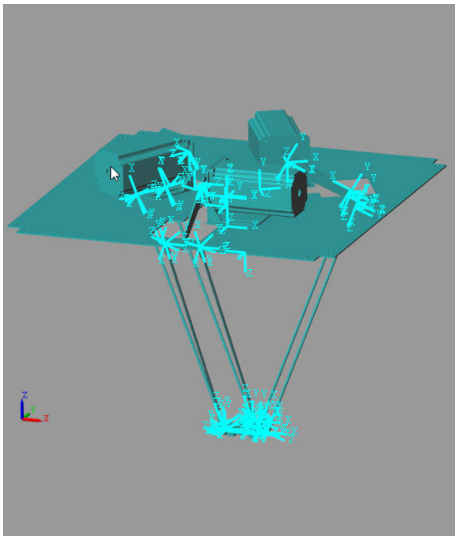

FIGURE 5. Delta robot simmechanic model created in Solidworks/Matlab/SimScape/Multibody model.

radius b have an intersection that describes position of end effector. Two solutions will be obtained but according to [41], only one of them could be acceptable.

C. DYNAMIC OF DELTA ROBOT

In this part, using Euler-Lagrange method, dynamic model of Delta parallel robot is determined. Euler-Lagrange differential equation is as follows:

$$\frac{d}{dt}\left(\frac{\partial L}{\partial \dot{q}_i}\right) - \frac{\partial L}{\partial q_i} = Q_i + \sum_{j=1}^{n_r} \lambda_j \frac{df_j}{\partial q_i} \quad for\ i = 1, 2, \ldots, n, \tag{5}$$

where j, q_i, i, n_r and n are restriction index, generalized coordinate i, generalized coordinate index, restrictions number and generalized coordinate number, respectively. In the above equation, L denotes Lagrangian and λ_j denotes Lagrange coefficients. The kinematic restriction formulas are defined as f_i and the generalized external force is $Q_i = \hat{Q}_i + \tau_i$; in which $\hat{Q}_i$ and τ_i are generalized external forces at end effector and applied torque in joint i, respectively. For the given trajectory 1, estimated values of X using PSO algorithm are shown in Table 1. To achieve equations of motion, Eq. (5) is rewritten in two separate parts. The first part includes uncertain Lagrange coefficients as follows:

$$\sum_{j=1}^{n_r} \lambda_j \frac{df_j}{dq_i} = \frac{d}{dt}\left(\frac{dL}{dq_i}\right) - \frac{dL}{dq_i}\hat{Q}_i \tag{6}$$

By obtaining Lagrange coefficients λ_j from Eq. (6), the second part can be calculated as follows:

$$Q_i = \frac{d}{dt}\left(\frac{dL}{dq_i}\right) - \frac{dL}{dq_i} = \sum_{j=1}^{n_r} \lambda_j \frac{df_j}{dq_i} \quad for\ i = n_r + 1, n_r + 2, \ \ldots, \ n. \tag{7}$$

q_i consists of six variables that the first three variables are related to spatial position and the second three variables are related to joint space θ_i. q_i is defined as follows:

$$q_i = [x,\ y,\ z,\ \theta_1,\ \theta_2\ , \theta_3] \quad with\ \ i = 1, 2, \ldots, 6. \tag{8}$$

As mentioned in the previous sections, the kinematics of Delta parallel robot has created some restrictions. From Eq. (1), the kinematic restrictions for the Lagrange equation is defined as:

$$\begin{cases} x_i = \cos(\phi_i)\,(r_c + a\cos(\theta_i))\,, \\ y_i = \sin(\phi_i)\,(r_c + a\cos(\theta_i))\,, \quad for\ i = 1, 2, 3, \\ z_i = a\sin(\theta_i)\,, \end{cases} \tag{9}$$

where $r_c = r_a - r_b$.

The difference between potential energy V and kinetic energy T is called Lagrange function L, which is defined as follows:

$$L = T - V. \tag{10}$$

Kinetic energy T for Delta parallel robot is defined as sum of a number of kinetic energies as follows:

$$T = T_c + \sum_{i=1}^{3} T_{ai} + T_{bi}, \tag{11}$$

where T_c, T_{ai} and T_{bi} with $i = 1, 2, 3$, denote kinetic energy of end effector, upper and lower arms, respectively. The potential energy V is defined as sum of several potential energies as follows:

$$V = V_c + \sum_{i=1}^{3} V_{ai} + V_{bi}. \tag{12}$$

Similarly, V_c, V_{ai} and V_{bi} denote the potential energy of end effector, upper and lower arms, respectively. In Eq. (6), the Lagrange coefficients that are unknown can be determined using following equation:

$$\begin{aligned} &2\sum_{i=1}^{3} \lambda_i \cos(\phi_i)\,(x + r_a - r_b {-} a\cos(\theta_i)) \\ &\quad = (m_n + 3\,m_b)\,\ddot{x} - f_{px} \\ &\qquad \times 2\sum_{i=1}^{3} \lambda_i \sin(\phi_i)\,(x + r_a - r_b {-} a\cos(\theta_i)) \\ &\quad = (m_n + 3\,m_b)\,\ddot{y} - f_{py} \\ &\qquad \times 2\sum_{i=1}^{3} \lambda_i\,(z {-} a\cos(a_i)) \\ &\quad = (m_n + 3m_b)\,\ddot{z} + (m_n + 3m_b)\,g - f_{pz}, \end{aligned} \tag{13}$$

where m_n, m_a and m_b are mass of end effector, upper and lower arms, respectively. g and $[\ddot{x}, \ddot{y}, \ddot{z}]$ are acceleration of gravitational and end effector, respectively. $[f_{px}, f_{py}, f_{pz}]$ denotes external forces applied to end effector.

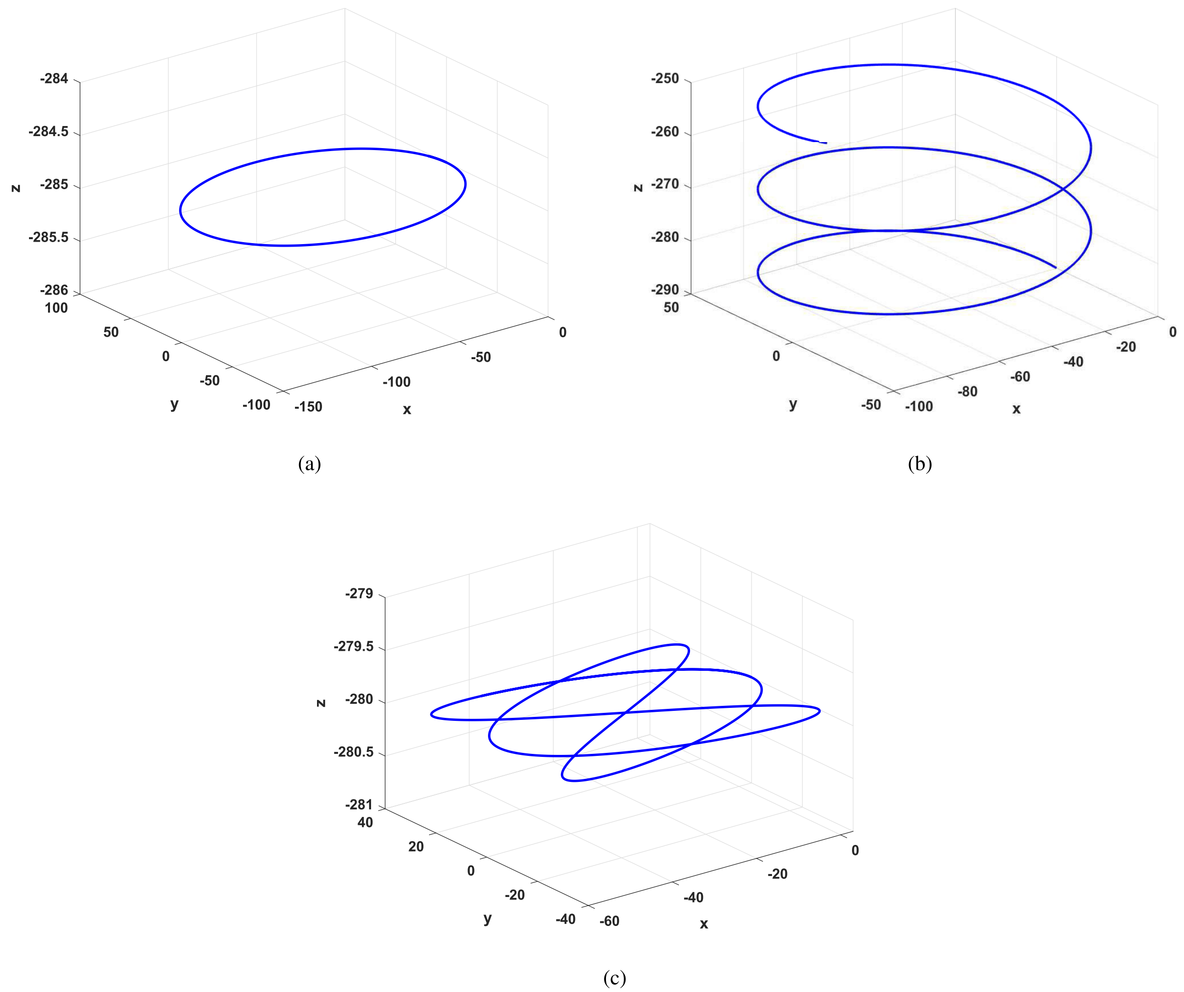

FIGURE 6. Trajectories for delta parallel robot. (a) : trajectory 1, (b): trajectory 2, (c): trajectory 3.

If Lagrange coefficients and motor inertia are obtained, the torque τ_i applying to joints are calculable from Eq. (6) as follows:

$$\begin{aligned}
\tau_1 &= \ddot{a}_1\left(I_m + \frac{1}{3}m_a a^2\right) + a\,g\cos(\theta_1) \\
&\quad \times \left(\frac{1}{2}m_a + m_b\right) - 2\lambda_1[\sin(\theta_1)\,(x\cos(\phi_1) \\
&\quad + y\cos(\phi_1) + r_a - r_b) - z\cos(\theta_1)] \\
\tau_2 &= \ddot{a}_2\left(I_m + \frac{1}{3}m_a a^2 + m_b a^2\right) + a\,g\cos(\theta_2) \\
&\quad \times \left(\frac{1}{2}m_a + m_b\right) - 2\lambda_2[\sin(\theta_2)\,(x\cos(\phi_2) \\
&\quad + y\cos(\phi_2) + r_a - r_b) - z\cos(\theta_2)] \\
\tau_3 &= \ddot{a}_3\left(I_m + \frac{1}{3}m_a a^2\right) + a\,g\cos(\theta_3) \\
&\quad \times \left(\frac{1}{3}m_a + m_b\right) - 2\lambda_3[\sin(\theta_3)\,(x\cos(\phi_3) \\
&\quad + y\cos(\phi_3) + r_a - r_b) - z\cos(\theta_3)]
\end{aligned} \tag{14}$$

A Solidworks/Matlab/SimScape/Multibody model is created for analyzing dynamic behavior and recognizing friction and inertia effects of mechanical model. To create Delta robot in Solidworks, all parts of it are designed and then these components are combined in assembly Solidworks and finally, the model is exported to Simulink in Matlab. Fig. 5 shows Delta robot model in mechanic explorer of Matlab. As can be seen in the figure, the gravitational acceleration is aligned with z-axis.

III. ESTIMATION OF DYNAMIC MODEL PARAMETERS OF DELTA ROBOT

In this section, trajectory generation for tracking and parameter estimation for dynamic model are described.

A. TRAJECTORY GENERATION

The Cartesian trajectory is generated with path planning for actual joints to the end effector which is tracked with constant velocity and acceleration. After generating, the proposed

Cartesian trajectories are given to the inverse kinematic (Eq. (3)).

The reference trajectories of the delta robot are spirals using the following equations:

$$\text{trajectory 1:}\quad \begin{cases} x = -70 + 70cos(t) \\ y = 75sin(t) \\ z = -285 \end{cases}$$

$$\text{trajectory 2:}\quad \begin{cases} x = -50 + 50cos(t) \\ y = 50sin(t) \\ z = -290 + 2.5t \end{cases}$$

$$trajectory3:\quad \begin{cases} x = -27 + 30cos(3t) \\ y = 30sin(2t) \\ z = -280 \end{cases}$$

Fig. 6 offers the trajectory 1, trajectory 2 and trajectory 3 in Cartesian coordinates. trajectory 1 is used in estimation of dynamic parameters. trajectory 2 and trajectory 3 are employed to validate proposed controller.

B. PSO ALGORITHM FOR PARAMETER ESTIMATION

Here, at first, dynamic parameterization of Delta robot is performed, and then the parameters of dynamic model are estimated with PSO algorithm.

For estimation of dynamic parameters, Eq. (14) is simplified as follows:

$$\begin{cases} \tau_1 = X_1\ddot{\theta}_1 - \sin(\theta_1)(X_2x + X_3y - X_6)+ \\ \cos(\theta_1)(X_4z + X_5) \\ \tau_2 = X_1\ddot{\theta}_2 - \sin(\theta_2)(X_7x + X_8y - X_{10})+ \\ \cos(\theta_2)(X_9z + X_5) \\ \tau_3 = X_1\ddot{\theta}_3 - \sin(\theta_3)(X_{11}x + X_{12}y - X_{14})+ \\ \cos(\theta_3)(X_{13}z + X_5) \end{cases} \tag{15}$$

where:

$$\begin{aligned}
&X_1 = I_m + \frac{1}{3}m_a a^2 + m_b a^2 \quad X_8 = 2\lambda_2 \sin(\phi_2) \\
&X_2 = 2\lambda_1 \cos(\phi_1) \quad X_9 = 2\lambda_2 \\
&X_3 = 2\lambda_1 \sin(\phi_1) \quad X_{10} = 2\lambda_2(r_b - r_a) \\
&X_4 = 2\lambda_1 \quad X_{11} = 2\lambda_3 \cos(\phi_3) \\
&X_5 = (\frac{1}{2}m_a + m_b)ag \quad X_{12} = 2\lambda_3 \sin(\phi_3) \\
&X_6 = 2\lambda_1(r_b - r_a) \quad X_{13} = 2\lambda_3 \\
&X_7 = 2\lambda_2 \cos(\phi_2) \quad X_{14} = 2\lambda_3(r_b - r_a)
\end{aligned}$$

To reduce complexity, Eq. (15) is rewritten in matrix form as follows:

$$\mathbf{Y}(\boldsymbol{\theta},\ \dot{\boldsymbol{\theta}},\ \ddot{\boldsymbol{\theta}})\mathbf{X} = \boldsymbol{\tau}, \tag{16}$$

where $\boldsymbol{\tau} = [\tau_1,\ \tau_2,\ \tau_3]^T$. $\mathbf{Y}(\boldsymbol{\theta},\ \dot{\boldsymbol{\theta}},\ \ddot{\boldsymbol{\theta}})$ is an $n_x \times r$ regression matrix of position, velocity, joint and space acceleration along with torque measured from the SimScape multibody model which is as follows:

TABLE 1. Estimated constant parameters of dynamic model.

parameter	value	parameter	value
X_1	0.0417	X_8	-0.0060
X_2	-0.0046	X_9	2.9028×10^{-4}
X_3	-0.0084	X_{10}	-0.0042
X_4	2.6723×10^{-4}	X_{11}	-0.0060
X_5	0.0346	X_{12}	0.0032
X_6	0.0190	X_{13}	4.7392×10^{-4}
X_7	0.0052	X_{14}	0.0210

$$\begin{bmatrix} y_{11} & y_{12} & \cdots & y_{114} \\ y_{21} & y_{22} & \cdots & y_{214} \\ y_{31} & y_{32} & \cdots & y_{314} \end{bmatrix},$$

where:

$$\begin{aligned}
&y_{11} = \ddot{\theta}_1 \quad y_{21} = \ddot{\theta}_2 \quad y_{31} = \ddot{\theta}_3 \\
&y_{12} = -x\sin(\theta_1) \quad y_{25} = \cos(\theta_2) \quad y_{35} = \cos(\theta_3) \\
&y_{13} = -y\sin(\theta_1) \quad y_{27} = -x\sin(\theta_2) \quad y_{311} = -x\sin(\theta_3) \\
&y_{14} = z\cos(\theta_1) \quad y_{28} = -y\cos(\theta_2) \quad y_{312} = -y\cos(\theta_3) \\
&y_{15} = \cos(\theta_1) \quad y_{29} = z\cos(\theta_2) \quad y_{313} = z\cos(\theta_3) \\
&y_{16} = \sin(\theta_1) \quad y_{210} = \sin(\theta_2) \quad y_{314} = \sin(\theta_3) \\
&y_{17} = y_{18} = 0 \quad y_{22} = y_{23} = 0 \quad y_{32} = y_{33} = 0 \\
&y_{19} = y_{110} = 0 \quad y_{24} = y_{26} = 0 \quad y_{34} = y_{36} = 0 \\
&y_{111} = y_{112} = 0 \quad y_{211} = y_{212} = 0 \quad y_{37} = y_{38} = 0 \\
&y_{113} = y_{114} = 0 \quad y_{213} = y_{214} = 0 \quad y_{39} = y_{310} = 0.
\end{aligned}$$

$\mathbf{X} = [X_1,\ X_2,\ \ldots,\ X_{14}]^T$ is a vector that includes unknown parameters of Delta robot.

In PSO algorithm, parameter estimation is performed by searching suitable values in parameter space. The methodology for Delta robot identification has been depicted in Fig. 9. As can be seen in the figure, for parameter estimation, it is necessary to minimize error between the measurement and computed torque related to a given trajectory. At each final time (t_f), all elements of X are updated. By minimizing following error cost function, optimal value of X is obtained.

$$E(k) = \frac{1}{N}\sum_{i=1}^{N}\sqrt{e_1(i)^2 + e_2(i)^2 + e_3(i)^2}, \tag{17}$$

where $e_1(i)$, $e_2(i)$ and $e_3(i)$ are errors between the measurement and computed torques of i-th sample for the first, second and third joints, respectively. N and k are number of samples and iteration number, respectively. For the given trajectory 1, estimated values of X using PSO algorithm are shown in Table 1.

IV. FRACTIONAL-ORDER SLIDING MODE CONTROL SCHEME

Delta robot is a nonlinear system whose parameters are affected by a number of factors. In order to achieve good performance in presence of uncertainties and disturbances, a robust controller is required. Many integer-order sliding

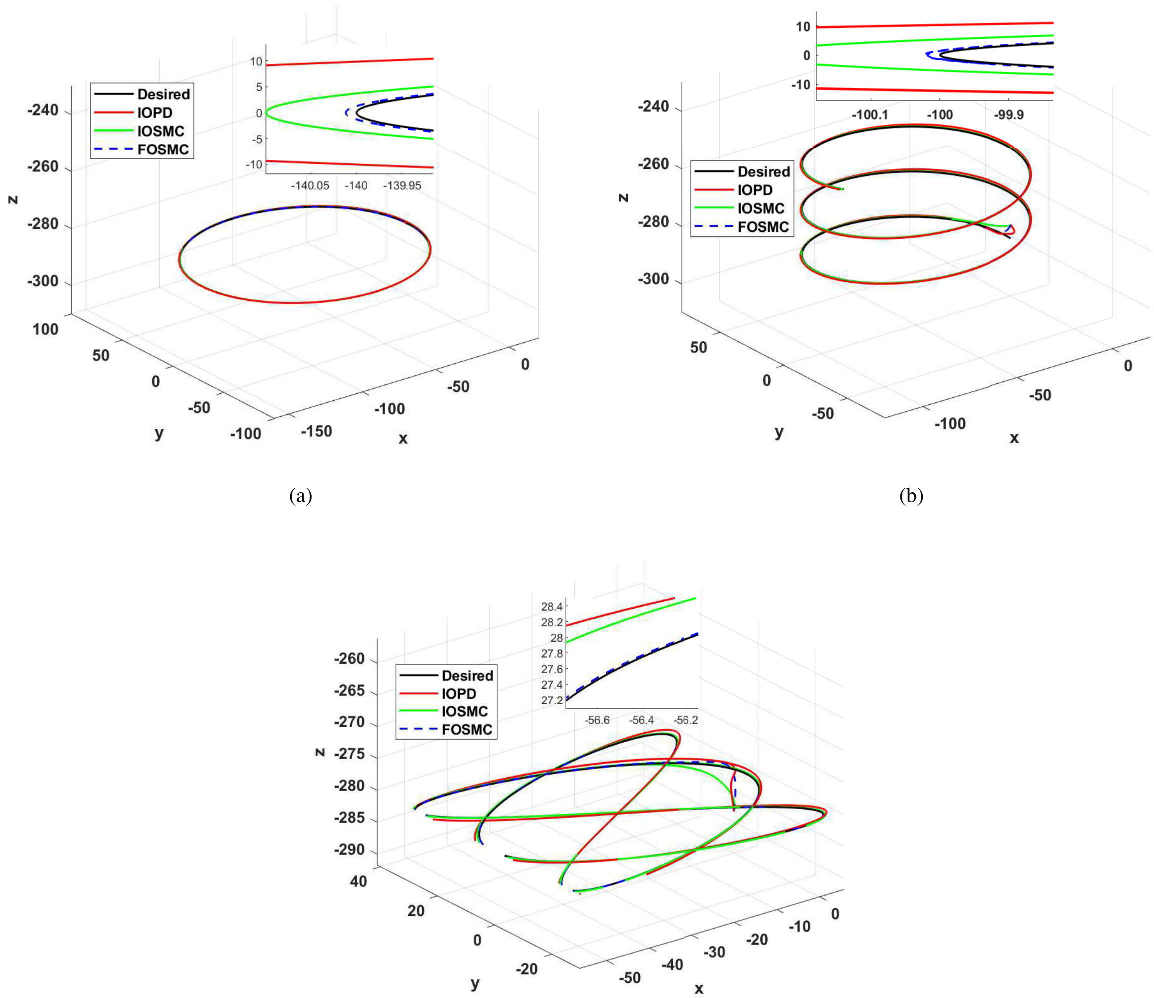

FIGURE 7. Trajectory tracking response for (a) : path1, (b): path2 and (c): path3.

mode controllers have been proposed in the literature. Fractional-order differential equations which are an expansion of integer-order differential equations can explain more accurately the dynamics of the system. In this regard, a Fractional-Order Sliding Mode Controller is proposed for Delta robot. Eq. (15) can be written as:

$$\mathbf{M}(\boldsymbol{\theta})\ddot{\boldsymbol{\theta}} + \mathbf{C}(\boldsymbol{\theta}, \dot{\boldsymbol{\theta}})\dot{\boldsymbol{\theta}} + \mathbf{G}(\boldsymbol{\theta}) = \boldsymbol{\tau}, \tag{18}$$

where $\boldsymbol{\theta}$, $\dot{\boldsymbol{\theta}}$, $\ddot{\boldsymbol{\theta}}$ are the angles, velocities and accelerations of actual joints, respectively. $\boldsymbol{\tau}$ is the applied torque, $\mathbf{M}(\boldsymbol{\theta})$ is the matrix of inertia, $\mathbf{C}(\boldsymbol{\theta}, \dot{\boldsymbol{\theta}})$ is the coriolis matrix and $\mathbf{G}(\boldsymbol{\theta})$ is gravity matrix.

The actual and nominal models are not the same in most cases; Therefore, due to outside interference, dynamics parameter uncertainty, and other system uncertainty factors, Eq. (18) will be updated by adding the model perturbation terms as follows:

$$\hat{\mathbf{M}}(\boldsymbol{\theta})\ddot{\boldsymbol{\theta}} + \hat{\mathbf{C}}(\boldsymbol{\theta}, \dot{\boldsymbol{\theta}})\dot{\boldsymbol{\theta}} + \hat{\mathbf{G}}(\boldsymbol{\theta}) + \boldsymbol{\tau_d} = \boldsymbol{\tau}, \tag{19}$$

where $\hat{\mathbf{M}}(\boldsymbol{\theta}) = \mathbf{M}(\boldsymbol{\theta}) - \mathbf{M_e}(\boldsymbol{\theta})$, $\hat{\mathbf{C}}(\boldsymbol{\theta}, \dot{\boldsymbol{\theta}})\dot{\boldsymbol{\theta}} = \mathbf{C}(\boldsymbol{\theta}, \dot{\boldsymbol{\theta}})\dot{\boldsymbol{\theta}} - \mathbf{C_e}(\boldsymbol{\theta}, \dot{\boldsymbol{\theta}})\dot{\boldsymbol{\theta}}$, and $\hat{\mathbf{G}}(\boldsymbol{\theta}) = \mathbf{G}(\boldsymbol{\theta}) - \mathbf{G_e}(\boldsymbol{\theta})$,

$\mathbf{M_e}(\boldsymbol{\theta})$, $\mathbf{C_e}(\boldsymbol{\theta}, \dot{\boldsymbol{\theta}})$ and $\mathbf{G_e}(\boldsymbol{\theta})$ represent the errors between the actual model and the nominal model caused by uncertainty of model parameters, while $\boldsymbol{\tau_d}$ represents the external disturbance term.

By applying fractional sliding mode control, the response is separated into two parts: first; signals can reach the sliding surface and second; they can slide and remain on the sliding surface. Prior to reach the sliding surface, the system gets affected by disturbances, noise and uncertainties in its parameters. Here, the fractional order sliding surfaces are

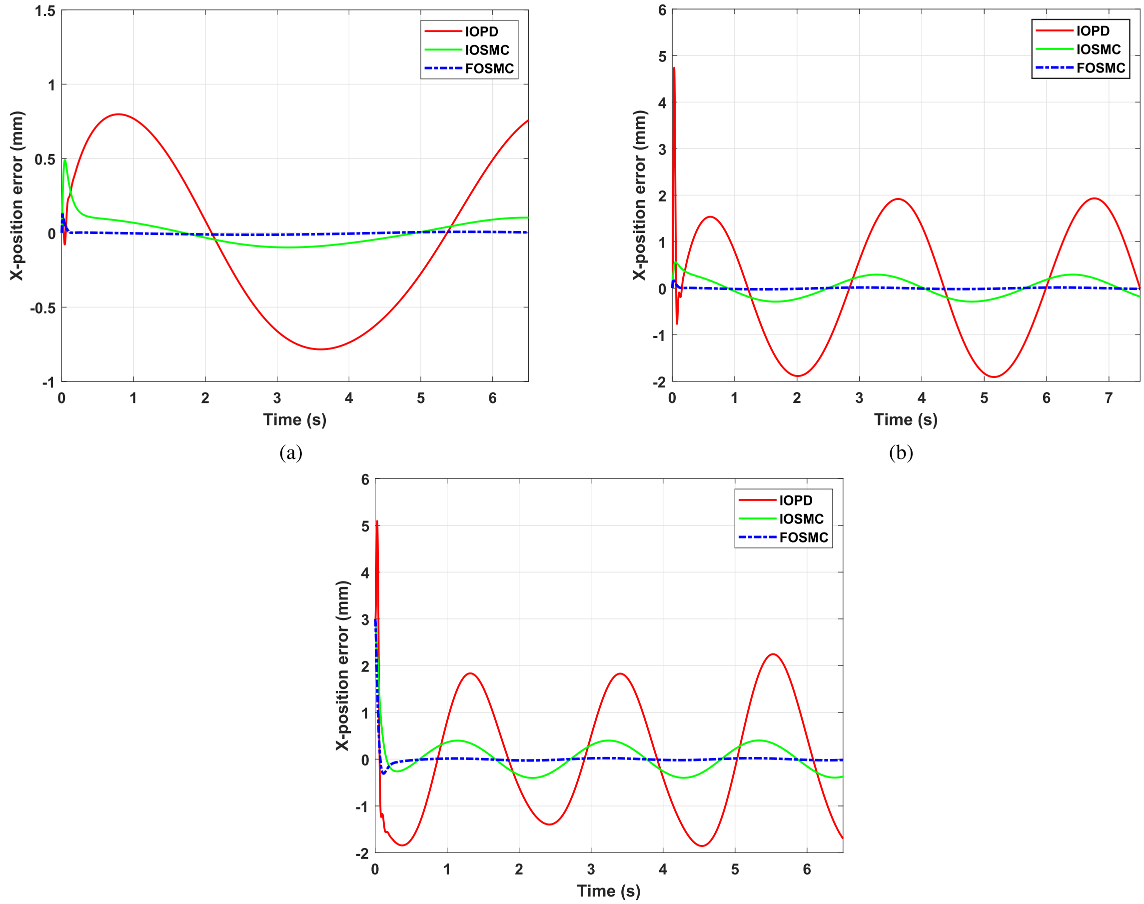

(a) (b) (c)

FIGURE 8. Position error (x-axis component) for (a) : trajectory 1, (b): trajectory 2 and (c): trajectory 3.

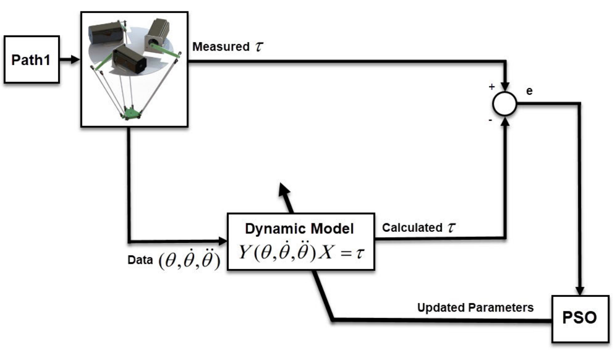

FIGURE 9. The methodology for parameter estimation of delta robot.

chosen as follows:

$$\mathbf{s(t)} = \begin{bmatrix} s_1 \\ s_2 \\ s_3 \end{bmatrix} = \mathbf{e}(\dot{t}) + D^{\alpha}\mathbf{e(t)} + \mathbf{K_p e(t)} = \dot{\boldsymbol{\theta}} - \dot{\boldsymbol{\theta}}_d + D^{\alpha}\mathbf{e(t)} + \mathbf{K_p e(t)} \tag{20}$$

where $\boldsymbol{\theta}_d$ denotes the reference joint trajectory, $\mathbf{e} = \boldsymbol{\theta} - \boldsymbol{\theta}_d$ denotes the tracking joint position error, $\mathbf{K_p} = diag[k_{p1},\ k_{p2},\ k_{p3}]$ is a diagonal matrix and k_{p1}, k_{p2} and k_{p3} are constants greater than zero. The Caputo fractional derivative of order $0 < \alpha < 1$ [42], is defined as follows:

$$D^{\alpha}\, e(t) = \frac{1}{\Gamma(1-\alpha)} \int_0^t (t-s)^{-\alpha}\, e'(s)ds \tag{21}$$

So:

$$\begin{aligned} \dot{\mathbf{s}} &= \ddot{\theta}_d - \ddot{\theta} + \mathbf{K_p}\dot{\mathbf{e}} + D^{\alpha+1}\mathbf{e} \\ &= \ddot{\theta}_d - \hat{\mathbf{M}}^{-1}\Big[-\boldsymbol{\tau} - \hat{\mathbf{C}}\dot{\boldsymbol{\theta}} - \hat{\mathbf{G}} - \boldsymbol{\tau}_d\Big] \\ &\quad + \mathbf{K_p}\dot{\mathbf{e}} + D^{\alpha+1}\mathbf{e} \end{aligned} \tag{22}$$

For purpose of stabilizing the parallel robot system, the controller for Delta robot system can be defined as:

$$\begin{aligned} \boldsymbol{\tau} &= \mathbf{M}\ddot{\theta}_d + \mathbf{C}\dot{\theta}_d + \mathbf{G} \\ &\quad + \mathbf{M}\Big(D^{\alpha+1}\mathbf{e} + \mathbf{K_p}\dot{\mathbf{e}}\Big) + \mathbf{C}\Big(D^{\alpha}\mathbf{e} + \mathbf{K_p e}\Big) \\ &\quad + \mathbf{K}_{sl}\mathbf{s} + \begin{bmatrix} n_1 sign(s_1) \\ n_2 sign(s_2) \\ n_3 sign(s_3) \end{bmatrix} \end{aligned} \tag{23}$$

where $\mathbf{K}_{sl}$ is a positive-definite matrix, and n_1, n_2 and n_3 are constant values.

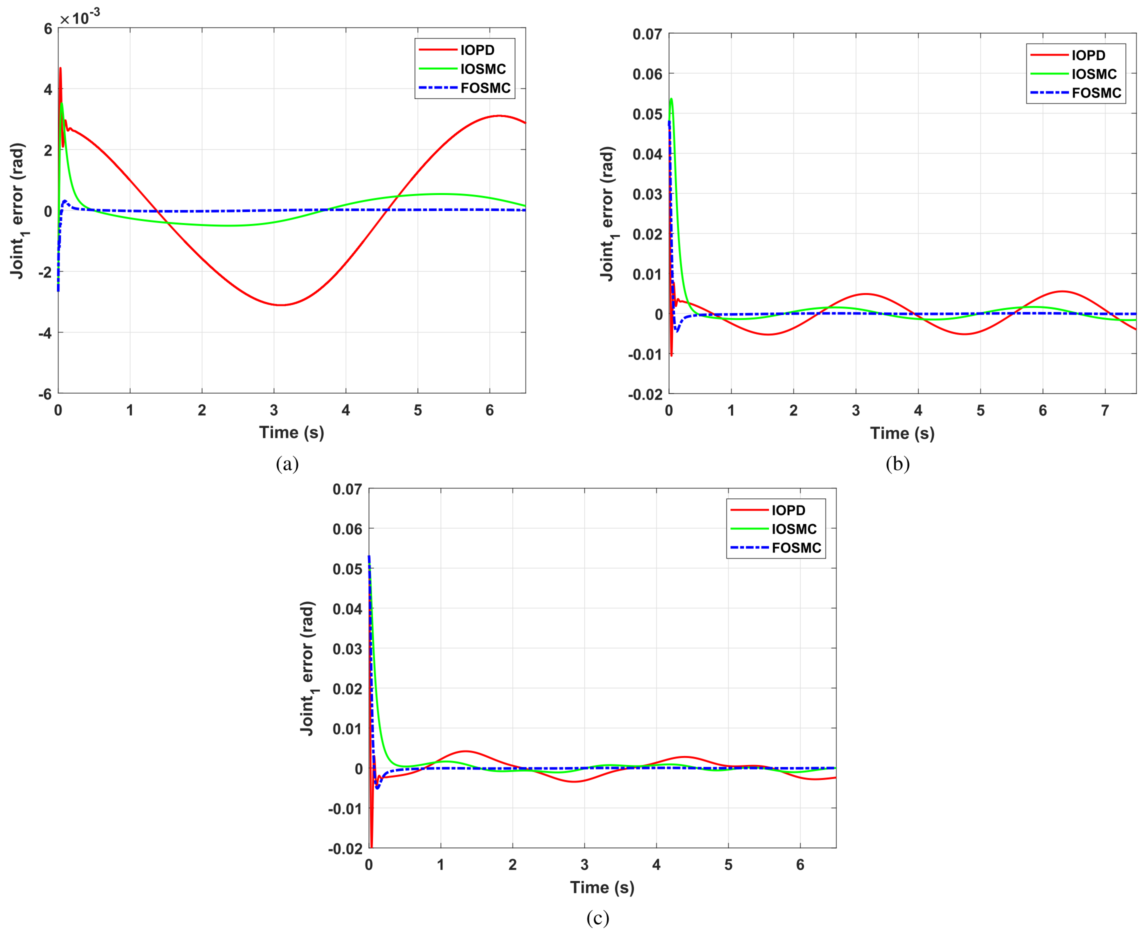

FIGURE 10. Error in joint 1 for (a) : trajectory 1, (b): trajectory 2 and (c): trajectory 3.

In order to ensure the convergence of the robot system, candidate Lyapunov function is defined as follows:

$$V = \frac{1}{2}\mathbf{s}^T\hat{\mathbf{M}}(\boldsymbol{\theta})\mathbf{s}, \tag{24}$$

By deriving the Lyapunov function, following relation can be obtained:

$$\begin{aligned}\dot{V} &= \mathbf{s}^T\hat{\mathbf{M}}(\boldsymbol{\theta})\dot{\mathbf{s}} + \frac{1}{2}\mathbf{s}^T\dot{\hat{\mathbf{M}}}(\boldsymbol{\theta})\mathbf{s} \\ &= \mathbf{s}^T\hat{\mathbf{M}}(\boldsymbol{\theta})\dot{\mathbf{s}} + \frac{1}{2}\mathbf{s}^T\left(\dot{\hat{\mathbf{M}}}(\boldsymbol{\theta})\mathbf{s} - 2\hat{\mathbf{C}}(\boldsymbol{\theta},\dot{\boldsymbol{\theta}})\right)\mathbf{s} \\ &\quad + \mathbf{s}^T\hat{\mathbf{C}}(\boldsymbol{\theta},\dot{\boldsymbol{\theta}})\mathbf{s}\end{aligned} \tag{25}$$

By using the skew-symmetric property of $\dot{\hat{\mathbf{M}}}(\boldsymbol{\theta})\mathbf{s} - 2\hat{\mathbf{C}}(\boldsymbol{\theta},\dot{\boldsymbol{\theta}})$, the following equation can be obtained:

$$\dot{V} = \mathbf{s}^T\left(\hat{\mathbf{M}}(\boldsymbol{\theta})\dot{\mathbf{s}} + \hat{\mathbf{C}}(\boldsymbol{\theta},\dot{\boldsymbol{\theta}})\mathbf{s}\right) \tag{26}$$

Substituting Eq. (22) in the above equation results in:

$$\begin{aligned}\dot{V} &= \mathbf{s}^T\Big[\hat{\mathbf{M}}\Big[-\mathbf{M}^{-1}(\boldsymbol{\tau} - \hat{\mathbf{C}}\dot{\boldsymbol{\theta}} - \hat{\mathbf{G}} - \boldsymbol{\tau}_d) + \ddot{\theta}_d \\ &\quad + D^{\alpha+1}\mathbf{e} + \mathbf{K_p}\dot{\mathbf{e}}\Big] + \hat{\mathbf{C}}\mathbf{s}\Big] = \mathbf{s}^T\Big[-\boldsymbol{\tau} + \hat{\mathbf{C}}\dot{\boldsymbol{\theta}} + \hat{\mathbf{G}} \\ &\quad + \boldsymbol{\tau}_d + (\mathbf{M} - \mathbf{M}_e)\left(\ddot{\theta}_d + D^{\alpha+1}\mathbf{e} + \mathbf{K_p}\dot{\mathbf{e}}\right) \\ &\quad + (\mathbf{C} - \mathbf{C}_e)\Big[\dot{\theta}_d - \dot{\theta} + D^{\alpha}\mathbf{e} + \mathbf{K_p}\mathbf{e}\Big]\Big]\end{aligned} \tag{27}$$

By simplifying the above equation, the following equation can be obtained:

$$\begin{aligned}\dot{V} = \mathbf{s}^T\Big[&-\boldsymbol{\tau} + \mathbf{M}\ddot{\theta}_d + \mathbf{M}D^{\alpha+1}\mathbf{e} + \mathbf{M}\mathbf{K_p}\dot{\mathbf{e}} \\ &+ \mathbf{G} + \boldsymbol{\tau}_d + \mathbf{C}\dot{\theta}_d + \mathbf{C}D^{\alpha}\mathbf{e} + \mathbf{C}\mathbf{K_p}\mathbf{e} \\ &- \mathbf{G}_e - \mathbf{M}_e\left(\ddot{\theta}_d + D^{\alpha+1}\mathbf{e} + \mathbf{K_p}\dot{\mathbf{e}}\right) \\ &- \mathbf{C}_e\left(\dot{\theta}_d + D^{\alpha}\mathbf{e} + \mathbf{K_p}\mathbf{e}\right)\Big]\end{aligned} \tag{28}$$

In the above equation, there are a number of terms caused by external disturbance and model errors which are denoted by $\mathbf{E}_{dis}$ as follows:

$$\begin{aligned}\mathbf{E}_{dis} = \mathbf{M}_e\ddot{\theta}_d + \mathbf{C}_e\dot{\theta}_d + \mathbf{G}_e - \boldsymbol{\tau}_d \\ + \mathbf{M}_e\left(D^{\alpha+1}\mathbf{e} + \mathbf{K_p}\dot{\mathbf{e}}\right) + \mathbf{C}_e\left(D^{\alpha}\mathbf{e} + \mathbf{K_p}\mathbf{e}\right)\end{aligned}$$

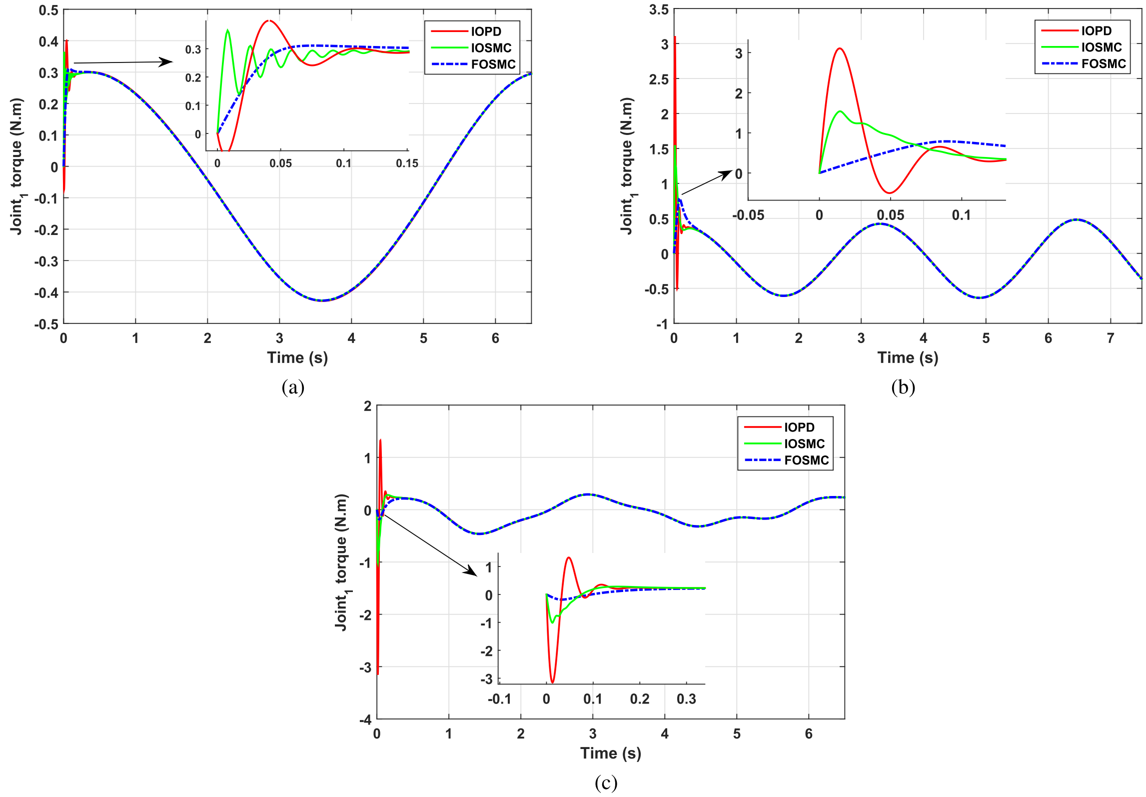

FIGURE 11. Applied torque to joint 1 for (a) : trajectory 1, (b): trajectory 2 and (c): trajectory 3.

Since disturbances are limited values, there is an upper bound for $\mathbf{E}_{dis}$ as follows:

$$|\mathbf{E}_{dis}| < \epsilon_i, \quad i \in \{1,2,3\}, \quad \epsilon_i > 0.$$

Eq. (28) can be simplified as:

$$\dot{V} = \mathbf{s}^T \Big[-\boldsymbol{\tau} - \mathbf{E}_{dis} + \mathbf{M}\ddot{\theta}_d + \mathbf{C}\dot{\theta}_d + \mathbf{G} + \mathbf{M}\Big(D^{\alpha+1}\mathbf{e} + \mathbf{K_p}\dot{\mathbf{e}}\Big) + \mathbf{C}\Big(D^{\alpha}\mathbf{e} + \mathbf{K_p}\mathbf{e}\Big)\Big] \tag{29}$$

by substituting Eq. (23) in the above equation, the following equation can be obtained:

$$\dot{V} = \mathbf{s}^T \left[-\mathbf{E}_{dis} - \mathbf{K}_{sl}\mathbf{s} - \begin{bmatrix} n_1 sign(s_1) \\ n_2 sign(s_2) \\ n_3 sign(s_3) \end{bmatrix} \right] \tag{30}$$

So, by assuming $n_i \geq \epsilon_i$, the following inequality holds:

$$\dot{V} \leq -\mathbf{s}^T \mathbf{K}_{sl}\mathbf{s} \leq 0 \tag{31}$$

According to the Lyapunov stability theory, the proposed controller can make trajectory-tracking errors converge to zero [43].

V. SIMULATION RESULTS

In this section, the performance of PD, SMC and FOSMC methods for trajectory tracking, according to their Root Mean Square (RMS) and Root Mean Square Error (RMSE) values for the position and joint errors, and the individual and global norms, mentioned in [44], are compared.

TABLE 2. Obtained parameters from PSO algorithm for PD, SMC, and FOSMC controllers.

Controller	k_p	k_d	α
FOSMC	68.2263	-	0.2327
SMC	10.3064	-	-
PD	81.6718	27.2603	-

Using PSO algorithm, the obtained parameters for PD, SMC, and FOSMC controllers are illustrated in Table 2.

Fig. 6 presents mentioned experiment trajectories for performance evaluation of PD, SMC and FOSMC controllers. Fig. 7 shows tracking response of moving plate of Delta robot when PD, SMC and FOSMC methods are utilized for three different trajectories. As can be seen in the figure, FOSMC method performs trajectory tracking much better than two other control strategies. Fig. 8 shows position error of moving plate of Delta robot for three trajectories when exploiting PD, SMC and FOSMC schemes. It can be seen that FOSMC has less position error than two other controllers. Also, the position error at the beginning of three test trajectories is less while FOSMC method is utilized which implies that FOSMC is able to overcome the initial inertia of Delta robot faster than two other control methods.

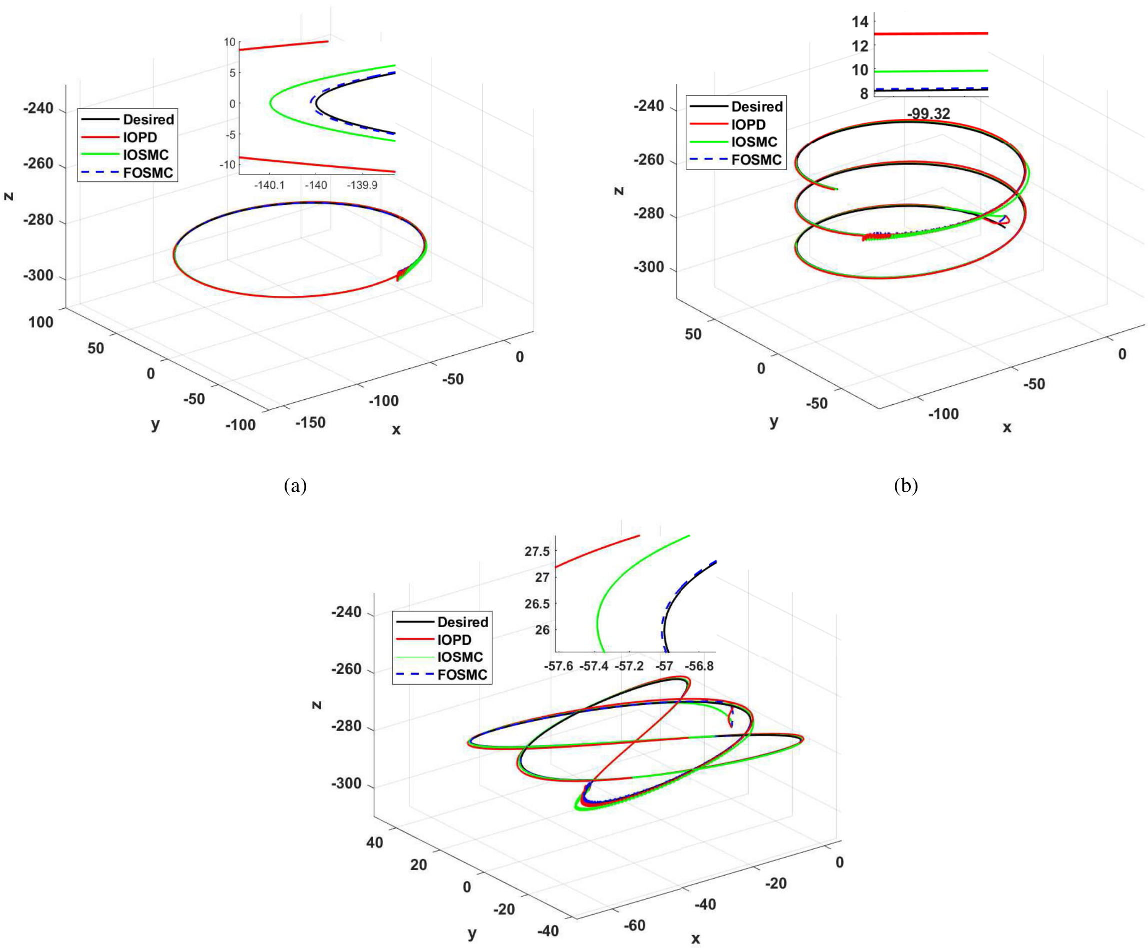

(a) (b) (c)

FIGURE 12. Trajectory tracking response with disturbance for (a) : trajectory 1, (b): trajectory 2 and (c): trajectory 3.

The actual joint errors for θ_1 are shown in Fig. 10, while exploiting PD, SMC and FOSMC methods. As can be seen in the figure, FOSMC method generates less error interval at the start of three trajectories. The response of FOSMC controller is smooth for actuator joint that shows superior control strategy when comparing with two other control methods. The applied torque signal to actual joint θ_1 for PD, SMC and FOSMC controllers is shown in Fig. 11. As can be seen in the figure, the control signal for three controllers is similar, but PD needs more torque to break the robot's initial inertia.

A. QUANTITATIVE ANALYSIS OF PD, SMC AND FOSMC METHODS

Specific performance indexes are used to quantify the performance of PD, SMC and FOSMC schemes. The RMSE is used for actual joint and position errors in trajectories. The value of RMSE is calculated as follows:

$$RMSE = \sqrt{\frac{1}{N}\sum_{i=0}^{N}(X_d(i) - X_a(i))^2}, \tag{32}$$

in which N returns the number of elements, $X_d(i)$ is desired value and $X_a(i)$ denotes the obtained value from Solidworks/Matlab/SimScape/Multibody simulation model at the instant i.

The RMS torque value is used for performance comparison in trajectories. The RMS torque value is calculated as follows:

$$\tau_{RMS} = \sqrt{\frac{1}{N}\sum_{i=0}^{N}\tau(i)^2}, \tag{33}$$

where N returns the number of elements, and $\tau(i)$ denotes the obtained value from Solidworks/Matlab/SimScape/Multibody simulation model at the instant i. The mean value of applied torque is measured according to RMS torque equation. In order to evaluate the tracking performance of a joint in Delta robot, the individual tracking norm N is used which is defined as follows:

$$\|\theta_{1,2,3}\|_{Individual} = \sqrt{\frac{1}{N}\sum_{i=0}^{N}(\tilde{\theta}_{1,2,3}(i)^2 + \dot{\tilde{\theta}}_{1,2,3}(i)^2)}, \tag{34}$$

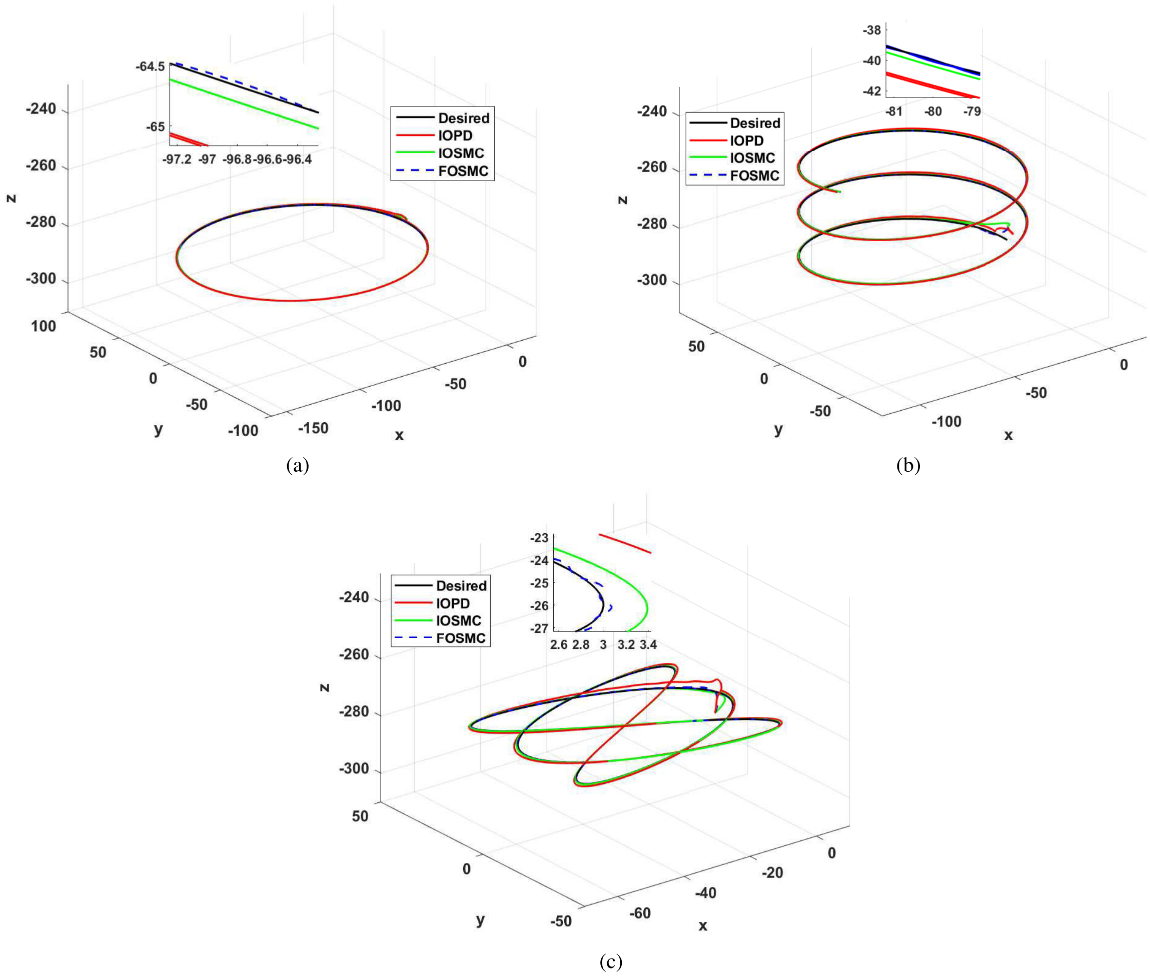

FIGURE 13. Trajectory tracking response with mass uncertainty for (a) : trajectory 1, (b): trajectory 2 and (c): trajectory 3.

where N returns the number of elements, $\tilde{\theta}_{1,2,3}(i)$ and $\dot{\tilde{\theta}}_{1,2,3}(i)$ are Delta parallel robot joint and joint velocity error at instant i, respectively. The trajectory tracking performance of Delta parallel robot is measured using trajectory tracking global norm as follows:

$$\|X_{x,y,z}\|_{Global} = \sqrt{\frac{1}{N}\sum_{i=0}^{N}(\tilde{X}_{x,y,z}(i)^2 + \dot{\tilde{X}}_{x,y,z}(i)^2)}, \quad (35)$$

where N returns the number of elements. The position and velocity errors are denoted as $\tilde{X}_{x,y,z}(i)$ and $\dot{\tilde{X}}_{x,y,z}(i)$, respectively.

Performance indexes for PD, SMC and FOSMC methods are given in Table 3. As can be seen in the Table, for three trajectories, the RMSE values for SMC and FOSMC are similar at joints error. For position errors, the RMSE values for x and y coordinates of the moving plate are similar for both SMC and FOSMC controllers but the advantage of FOSMC controller is quite clear. For z coordinate, the value of RMSE for FOSMC controller is less than 50% of SMC controller. It can also be seen that using FOSMC controller, less torque is required to track all trajectories. At the end, individual and global norms for FOSMC controller have less value than other controllers, which shows superior performance of FOSMC method in tracking desired trajectories.

VI. ROBUSTNESS ANALYSIS

The robustness of PD, SMC and FOSMC controllers are evaluated in three different experiments i.e. applying disturbance to joint actuator of Delta parallel robot, applying random noise to the input of controllers and applying a critical payload to the moving plate. The performance indexes (32)-(35) are employed to evaluate performance of controllers in each experiment.

A. EVALUATING PERFORMANCE OF CONTROLLERS IN PRESENCE OF EXTERNAL DISTURBANCES

Here, the external disturbance which is defined as follows will be applied to all three robot joints.

$$d(t) = 1.5 \times 10^5 e^{-2t} \sin(500t). \quad (36)$$

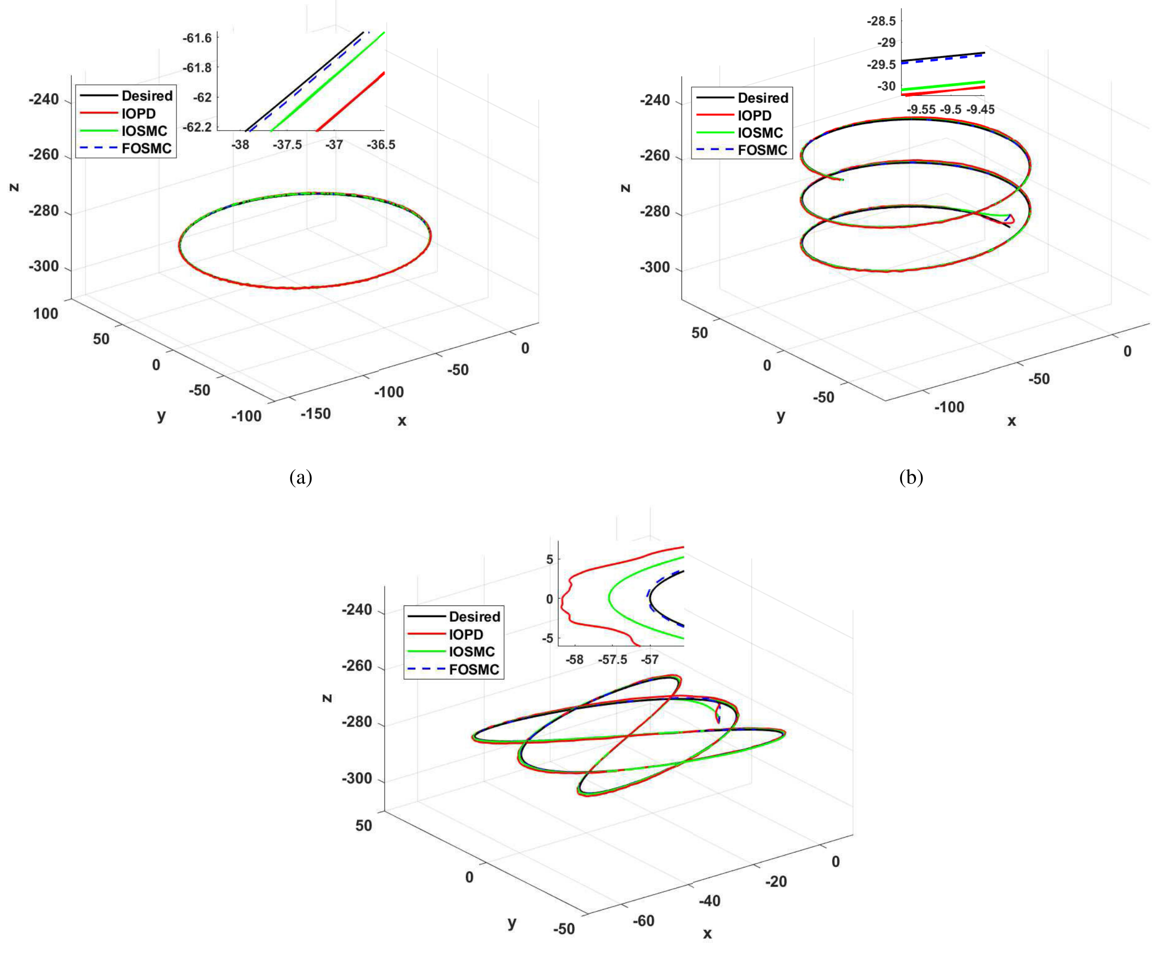

(a) (b) (c)

FIGURE 14. Tracking response with random noise for (a) : trajectory 1, (b): trajectory 2 and (c): trajectory 3.

TABLE 3. Performance indexes for PD, SMC and FOSMC methods.

Performance index	Signal	trajectory 1			trajectory 2			trajectory 3		
		$FOSMC$	SMC	PD	$FOSMC$	SMC	PD	$FOSMC$	SMC	PD
RMSE	θ_1	4.5376e-04	4.5335e-04	0.0021	0.0062	0.0065	0.0065	0.0024	0.0048	0.0032
	θ_2	4.8043e-04	4.9058e-04	0.0036	0.0062	0.0064	0.0113	0.0032	0.0064	0.0097
	θ_3	3.0034e-04	3.0021e-04	0.0011	0.0061	0.0062	0.0059	0.0020	0.0040	0.0029
	x	0.0722	0.0791	0.5714	0.1999	0.2918	1.5139	0.3017	0.3856	1.3514
	y	0.0911	0.1116	0.3013	0.2173	0.6810	0.6857	0.1224	0.1299	0.6806
	z	0.0262	0.0397	0.1266	0.6335	1.3993	0.5894	0.2313	0.5887	0.2967
RMS	τ_1	0.2518	0.2520	0.2527	0.4068	0.5383	0.5440	0.2110	0.2974	0.2798
	τ_2	0.3623	0.3631	0.3649	0.4551	0.5778	0.4908	0.3514	0.4119	0.3809
	τ_3	0.1564	0.1587	0.1568	0.2720	0.4581	0.4706	0.2447	0.2486	0.2761
Individual norm	θ_1	0.0092	0.0135	0.0130	0.0991	0.3625	0.3697	0.1748	0.0386	0.1797
	θ_2	0.0030	0.0059	0.0064	0.0923	0.3712	0.1874	0.0492	0.2122	0.1102
	θ_3	0.0069	0.0074	0.0062	0.0975	0.3776	0.3911	0.0301	0.1225	0.1286
Global norm	x, y, z	2.0638	2.3286	2.4053	12.9005	38.8246	55.6835	20.0006	24.9487	23.4135

For all trajectories, this disturbance begins at $t = 5s$ and ends at $t = 6s$. Fig. 12c represents the response of trajectory tracking in presence of disturbance for PD, SMC and FOSMC controllers. It is clear that FOSMC method is faster than two other suggested controllers and it also has a disturbance rejection. The performance indexes (32)-(35) for PD, SMC

TABLE 4. Performance indexes for PD, SMC and FOSMC controllers in presence of external disturbance.

Performance index	Signal	trajectory 1			trajectory 2			trajectory 3		
		$FOSMC$	SMC	PD	$FOSMC$	SMC	PD	$FOSMC$	SMC	PD
RMSE	θ_1	0.0011	0.0023	0.0023	0.0063	0.0167	0.0067	0.0031	0.0060	0.0036
	θ_2	0.0011	0.0015	0.0038	0.0063	0.0139	0.0114	0.0038	0.0076	0.0098
	θ_3	0.0011	0.0015	0.0015	0.0063	0.0123	0.0060	0.0026	0.0053	0.0033
	x	0.0743	0.1682	0.5747	0.2040	0.6072	1.5165	0.3125	0.3871	1.3479
	y	0.0940	0.2790	0.3029	0.2182	1.1437	0.6854	0.1342	0.1309	0.6782
	z	0.1023	0.1605	0.1603	0.6436	1.4232	0.6001	0.2947	0.6110	0.3308
RMS	τ_1	0.2538	0.2528	0.2548	0.5406	0.4114	0.5466	0.2954	0.3857	0.3788
	τ_2	0.3640	0.3632	0.3658	0.5790	0.4573	0.4913	0.4268	0.3857	0.378
	τ_3	0.1590	0.1571	0.1601	0.4588	0.2726	0.4717	0.2849	0.3024	0.2803
Individual norm	θ_1	0.4698	0.4696	0.4707	0.5835	0.5880	0.6884	0.7418	0.8304	0.7362
	θ_2	0.4527	0.4529	0.4529	0.46132	0.5546	0.5795	0.7295	0.7973	0.6953
	θ_3	0.4646	0.4647	0.4655	0.5914	0.5880	0.7000	0.7308	0.8327	0.7276
Global norm	x, y, z	37.1089	47.1180	47.2165	48.0319	57.4787	78.9618	63.6561	81.3998	73.8806

TABLE 5. Performance indexes for PD, SMC and FOSMC controllers with mass uncertainty.

Performance index	Signal	trajectory 1			trajectory 2			trajectory 3		
		$FOSMC$	SMC	PD	$FOSMC$	SMC	PD	$FOSMC$	SMC	PD
RMSE	θ_1	4.2931e-04	3.8403e-04	0.0021	0.0070	0.0145	0.0074	0.0058	0.0061	0.0037
	θ_2	8.8897e-04	0.0013	0.0046	0.0067	0.0167	0.0120	0.0062	0.0068	0.0109
	θ_3	6.9599e-04	0.0015	0.0015	0.0073	0.0111	0.0072	0.0056	0.0053	0.0033
	x	0.1793	0.3279	0.7246	0.3611	0.9808	1.7308	0.3114	0.3204	1.54159
	y	0.0913	0.1000	0.4241	0.2934	0.2956	0.8342	0.1346	0.1321	0.7667
	z	0.0287	0.0317	0.1400	0.7171	1.4391	0.6356	0.2906	0.5880	0.3284
RMS	τ_1	0.3983	0.3980	0.3987	0.6604	0.5033	0.6823	0.3164	0.3814	0.4357
	τ_2	0.8928	0.8921	0.8930	0.9103	0.8240	0.8375	0.4450	0.7642	0.7824
	τ_3	0.3660	0.3650	0.3652	0.6367	0.4390	0.6706	0.3080	0.4069	0.4267
Individual norm	θ_1	0.0065	0.0159	0.0144	0.1001	0.4157	0.4109	7.0671	0.0377	0.1939
	θ_2	0.0218	0.0363	0.0259	0.0941	0.4075	0.2302	7.0684	0.0549	0.1463
	θ_3	0.0211	0.0289	0.0143	0.1050	0.4553	0.4549	7.0656	0.0331	0.1355
Global norm	x, y, z	5.3733	8.3800	5.2262	35.7761	48.4634	35.9881	25.0525	26.6910	25.7154

and FOSMC methods in presence of external disturbance which is applied to actual joints, are presented in Table 4. In FOSMC method, the value of RMSE for actual joint errors, is at least 60% less than two other proposed controllers. This is also true for RMSE related to position error in tracking all three trajectories that again confirms higher performance of FOSMC controller in presence of external disturbances. The experiment is conducted while the torque applied to the actuators is the same for all three controllers. Individual and global norms also indicate less value for FOSMC among three controllers in presence of external disturbance. From Table 4, it can be confirmed that FOSMC controller shows robustness against external disturbances.

B. EVALUATING PERFORMANCE OF CONTROLLERS WHILE APPLYING PAYLOAD

Here, the controllers' performance is evaluated in presence of critical payload of 0.5 kg on the moving plate to track three trajectories of the experiments. Trajectory tracking response of suggested controllers for all trajectories is illustrated in Fig. 13. As expected, FOSMC controller performs better than two other controllers. It should be noted that critical payload changes the dynamic parameters of Delta robot. Despite these conditions, FOSMC controller shows the best performance in trajectory tracking. The performance indexes (32)-(35) for PD, SMC and FOSMC methods with mass uncertainty of moving plate, are presented in Table 5. The results of RMSE for actual joints and position errors, as well as individual and global norms, show higher performance of FOSMC controller. The average amount of torque applied to this controller is a little higher, despite the mass uncertainty; But, since the controller has minimum tracking errors, it can still confirm that according to the Table 5, FOSMC controller is more robust against mass uncertainty in tracking various trajectories.

C. EVALUATING PERFORMANCE OF CONTROLLERS WHILE APPLYING RANDOM NOISE

In this section, random noise with a range of $\pm 0.5^\circ$ is applied to the input of controllers. Fig. 14 shows the effect of this noise on performance of controllers in which the fast response of FOSMC method and its stable performance is clear. According to Table 6, it can be announced that the RMSE error, individual and global norms in presence of random noise for FOSMC method, is the lowest among all controllers. The RMS of applied torque to this controller is

TABLE 6. Performance indexes for PD, SMC and FOSMC controllers with random noise.

Performance index	Signal	trajectory 1			trajectory 2			trajectory 3		
		$FOSMC$	SMC	PD	$FOSMC$	SMC	PD	$FOSMC$	SMC	PD
RMSE	θ_1	0.0051	0.0052	0.0056	0.0081	0.0172	0.0084	0.0058	0.0076	0.0061
	θ_2	0.0051	0.0052	0.0063	0.0081	0.0144	0.0124	0.0062	0.0089	0.0110
	θ_3	0.0051	0.0052	0.0053	0.0080	0.0132	0.0079	0.0056	0.0070	0.0592
	x	0.0832	0.1110	0.5854	0.2006	0.3772	1.5152	0.3114	0.3858	1.3561
	y	0.0950	0.1476	0.3137	0.2185	0.7752	0.6885	0.1346	0.1303	0.6857
	z	0.0542	0.0562	0.1759	0.5470	1.4282	0.5983	0.2906	0.5801	0.3126
RMS	τ_1	0.2714	0.2522	0.2827	0.6409	0.4081	0.5580	0.3164	0.2347	0.3039
	τ_2	0.3761	0.3627	0.3663	0.5859	0.4562	0.4916	0.4450	0.3625	0.3826
	τ_3	0.1861	0.1569	0.2034	0.4683	0.2728	0.4875	0.3080	0.2637	0.3017
Individual norm	θ_1	7.1705	7.1711	7.1714	7.1402	7.1492	7.1499	7.0645	7.0671	7.0666
	θ_2	7.1705	7.1711	7.1706	7.1401	7.1497	7.1420	7.0646	7.0684	7.0648
	θ_3	7.1705	7.1711	7.1714	7.1402	7.1500	7.1512	7.0645	7.0659	7.0656
Global norm	x, y, z	2.9429	9.4120	17.2281	13.7809	39.2478	57.7062	6.0525	20.4052	27.6996

slightly higher however the least errors in tracing various trajectories can be seen. As a result, it can be announced that the proposed FOSMC controller is also robust to random noise in the input of controllers.

VII. CONCLUSION

In this research, the effects of three different types of controllers i.e. PD, SMC and FOSMC, on error minimization of trajectory tracking of Delta parallel robot have been investigated. The proposed controllers have been designed with CTC technique. To estimate dynamic parameters and validate proposed controllers, a Solidworks/Matlab/SimScape/Multibody simulation model has been exploited. Dynamic parameterizations of delta robot have been performed and parameters of dynamic model have been estimated using PSO algorithm. The evaluations have been performed in presence of external disturbance, mass uncertainty and random noise. The results confirm that in all experiments, FOSMC method shows the best response and is more robust than other two controllers.

REFERENCES

[1] R. Jha, D. Chablat, L. Baron, F. Rouillier, and G. Moroz, "Workspace, joint space and singularities of a family of delta-like robot," *Mechanism Mach. Theory*, vol. 127, pp. 73–95, Sep. 2018.

[2] Z. Anvari, P. Ataei, and M. T. Masouleh, "Collision-free workspace and kinetostatic performances of a 4-DOF delta parallel robot," *J. Brazilian Soc. Mech. Sci. Eng.*, vol. 41, no. 2, p. 99, Feb. 2019.

[3] G. Aquino, J. D. J. Rubio, J. Pacheco, G. J. Gutierrez, G. Ochoa, R. Balcazar, D. R. Cruz, E. Garcia, J. F. Novoa, and A. Zacarias, "Novel nonlinear hypothesis for the delta parallel robot modeling," *IEEE Access*, vol. 8, pp. 46324–46334, 2020.

[4] C. E. Boudjedir, M. Bouri, and D. Boukhetala, "Iterative learning control for trajectory tracking of a parallel delta robot," *at-Automatisierungstechnik*, vol. 67, no. 2, pp. 145–156, Feb. 2019.

[5] J. Brinker, B. Corves, and Y. Takeda, "Kinematic performance evaluation of high-speed delta parallel robots based on motion/force transmission indices," *Mechanism Mach. Theory*, vol. 125, pp. 111–125, Jul. 2018.

[6] J. Brinker, N. Funk, P. Ingenlath, Y. Takeda, and B. Corves, "Comparative study of serial–parallel delta robots with full orientation capabilities," *IEEE Robot. Autom. Lett.*, vol. 2, no. 2, pp. 920–926, Apr. 2017.

[7] E. Idá, S. Briot, and M. Carricato, "Natural oscillations of underactuated cable-driven parallel robots," *IEEE Access*, vol. 9, pp. 71660–71672, 2021.

[8] L. Angel and J. Viola, "Fractional order PID for tracking control of a parallel robotic manipulator type delta," *ISA Trans.*, vol. 79, pp. 172–188, Aug. 2018.

[9] N. Van Khang, N. Q. Hoang, N. D. Sang, and N. D. Dung, "A comparison study of some control methods for delta spatial parallel robot," *J. Comput. Sci. Cybern.*, vol. 31, no. 1, pp. 71–81, 2015.

[10] M. Rachedi, M. Bouri, and B. Hemici, "Application of an H∞ control strategy to the parallel delta," in *Proc. CCCA*, 2012, pp. 1–6.

[11] R. Zhao, L. Wu, and Y.-H. Chen, "Robust control for nonlinear delta parallel robot with uncertainty: An online estimation approach," *IEEE Access*, vol. 8, pp. 97604–97617, 2020.

[12] M. Rachedi, "Model based control of 3 DOF parallel delta robot using inverse dynamic model," in *Proc. IEEE Int. Conf. Mechatronics Autom. (ICMA)*, Aug. 2017, pp. 203–208.

[13] G. Rigatos and P. Siano, "An H-infinity feedback control approach to autonomous robot navigation," in *Proc. 40th Annu. Conf. IEEE Ind. Electron. Soc. (IECON)*, Oct. 2014, pp. 2689–2694.

[14] C. E. Boudjedir, M. Bouri, and D. Boukhetala, "An enhanced adaptive time delay control-based integral sliding mode for trajectory tracking of robot manipulators," *IEEE Trans. Control Syst. Technol.*, vol. 31, no. 3, pp. 1042–1050, May 2023.

[15] S. Han, H. Wang, and Y. Tian, "Model-free based adaptive nonsingular fast terminal sliding mode control with time-delay estimation for a 12 DOF multi-functional lower limb exoskeleton," *Adv. Eng. Softw.*, vol. 119, pp. 38–47, May 2018.

[16] J. Baek, M. Jin, and S. Han, "A new adaptive sliding-mode control scheme for application to robot manipulators," *IEEE Trans. Ind. Electron.*, vol. 63, no. 6, pp. 3628–3637, Jun. 2016.

[17] H. Dong, X. Yang, and M. V. Basin, "Practical tracking of permanent magnet linear motor via logarithmic sliding mode control," *IEEE/ASME Trans. Mechatronics*, vol. 27, no. 5, pp. 4112–4121, Oct. 2022.

[18] S. Shi, S. Xu, B. Zhang, Q. Ma, and Z. Zhang, "Global second-order sliding mode control for nonlinear uncertain systems," *Int. J. Robust Nonlinear Control*, vol. 29, no. 1, pp. 224–237, Jan. 2019.

[19] F. Muñoz, E. S. Espinoza, I. González-Hernández, S. Salazar, and R. Lozano, "Robust trajectory tracking for unmanned aircraft systems using a nonsingular terminal modified super-twisting sliding mode controller," *J. Intell. Robot. Syst.*, vol. 93, nos. 1–2, pp. 55–72, Feb. 2019.

[20] Y. Wang, Y. Xia, H. Li, and P. Zhou, "A new integral sliding mode design method for nonlinear stochastic systems," *Automatica*, vol. 90, pp. 304–309, Apr. 2018.

[21] I. Jmel, H. Dimassi, S. Hadj-Said, and F. M'Sahli, "An adaptive sliding mode observer for inverted pendulum under mass variation and disturbances with experimental validation," *ISA Trans.*, vol. 102, pp. 264–279, Jul. 2020.

[22] X. Zhou, T. Wang, and D. Diallo, "An active disturbance rejection sensorless control strategy based on sliding mode observer for marine current turbine," *ISA Trans.*, vol. 124, pp. 403–410, May 2020.

[23] R. Hu, H. Deng, and Y. Zhang, "Novel dynamic-sliding-mode-manifold-based continuous fractional-order nonsingular terminal sliding mode control for a class of second-order nonlinear systems," *IEEE Access*, vol. 8, pp. 19820–19829, 2020.

[24] Z. Ma, Z. Liu, P. Huang, and Z. Kuang, "Adaptive fractional-order sliding mode control for admittance-based telerobotic system with optimized order and force estimation," *IEEE Trans. Ind. Electron.*, vol. 69, no. 5, pp. 5165–5174, May 2022.

[25] R. Stanisławski, M. Rydel, and Z. Li, "A new reduced-order implementation of discrete-time fractional-order PID controller," *IEEE Access*, vol. 10, pp. 17417–17429, 2022.

[26] J. Wang, C. Shao, and Y.-Q. Chen, "Fractional order sliding mode control via disturbance observer for a class of fractional order systems with mismatched disturbance," *Mechatronics*, vol. 53, pp. 8–19, Aug. 2018.

[27] A. Modiri and S. Mobayen, "Adaptive terminal sliding mode control scheme for synchronization of fractional-order uncertain chaotic systems," *ISA Trans.*, vol. 105, pp. 33–50, Oct. 2020.

[28] B. Yang, T. Yu, H. Shu, D. Zhu, N. An, Y. Sang, and L. Jiang, "Perturbation observer based fractional-order sliding-mode controller for MPPT of grid-connected PV inverters: Design and real-time implementation," *Control Eng. Pract.*, vol. 79, pp. 105–125, Oct. 2018.

[29] P. Zhu, Y. Chen, M. Li, P. Zhang, and Z. Wan, "Fractional-order sliding mode position tracking control for servo system with disturbance," *ISA Trans.*, vol. 105, pp. 269–277, Oct. 2020.

[30] S. Chávez-Vázquez, J. F. Gómez-Aguilar, J. E. Lavín-Delgado, R. F. Escobar-Jiménez, and V. H. Olivares-Peregrino, "Applications of fractional operators in robotics: A review," *J. Intell. Robot. Syst.*, vol. 104, no. 4, p. 63, Apr. 2022.

[31] J. Sun, J. Wang, P. Yang, and S. Guo, "Fractional-order prescribed performance sliding mode control with time delay estimation for wearable exoskeletons," *IEEE Trans. Ind. Informat.*, pp. 1–10, 2022.

[32] A. Van den Bos, *Parameter Estimation for Scientists and Engineers*. Hoboken, NJ, USA: Wiley, 2007.

[33] L. Zhang, J. Wang, J. Chen, K. Chen, B. Lin, and F. Xu, "Dynamic modeling for a 6-DOF robot manipulator based on a centrosymmetric static friction model and whale genetic optimization algorithm," *Adv. Eng. Softw.*, vol. 135, Sep. 2019, Art. no. 102684.

[34] J. Tao, B. Ye, Y. Xie, X. Tang, and B. Song, "Dynamic modeling and load identification of industrial robot using improved particle swarm optimization," in *Proc. IEEE/ASME Int. Conf. Adv. Intell. Mechatronics (AIM)*, Jul. 2018, pp. 75–80.

[35] R. V. Ram, P. M. Pathak, and S. J. Junco, "Inverse kinematics of mobile manipulator using bidirectional particle swarm optimization by manipulator decoupling," *Mechanism Mach. Theory*, vol. 131, pp. 385–405, Jan. 2019.

[36] H.-T. Hsieh and C.-H. Chu, "Improving optimization of tool path planning in 5-axis flank milling using advanced PSO algorithms," *Robot. Comput.-Integr. Manuf.*, vol. 29, no. 3, pp. 3–11, Jun. 2013.

[37] W. Wang, H. Song, Z. Yan, L. Sun, and Z. Du, "A universal index and an improved PSO algorithm for optimal pose selection in kinematic calibration of a novel surgical robot," *Robot. Comput.-Integr. Manuf.*, vol. 50, pp. 90–101, Apr. 2018.

[38] T. Ladhari, I. Khoja, F. Msahli, and A. Sakly, "Parameter identification of a reduced nonlinear model for an activated sludge process based on cuckoo search algorithm," *Trans. Inst. Meas. Control*, vol. 41, no. 12, pp. 3352–3363, 2019.

[39] R. Clavel, "Conception d'un robot parallele rapide a 4 degres de liberte," Ph.D. thesis, THESIS-925, EPFL, Lausanne, Switzerland, 1991.

[40] R. Clavel, "Device for the movement and positioning of an element in space," U.S. Patent 4 976 582, Dec. 11, 1990.

[41] L. Angel, J. Bermúdez, and O. Muñoz, "Dynamic optimization and building of a parallel delta-type robot," in *Proc. IEEE Int. Conf. Robot. Biomimetics (ROBIO)*, Dec. 2013, pp. 444–449.

[42] I. Podlubny, *Fractional Differential Equations: An Introduction to Fractional Derivatives, Fractional Differential Equations, to Methods of Their Solution and Some of Their Applications*. Amsterdam, The Netherlands: Elsevier, 1998, vol. 198.

[43] M. Qin, S. Dian, B. Guo, X. Tao, and T. Zhao, "Fractional-order SMC controller for mobile robot trajectory tracking under actuator fault," *Syst. Sci. Control Eng.*, vol. 10, no. 1, pp. 312–324, Dec. 2022.

[44] F. Reyes, *Robótica-Control de Robots Manipuladores*. Mexico: Alfaomega Grupo Editor, 2011.

BEHNOUSH ALIZADEH received the B.Sc. and M.Sc. degrees in mechatronic engineering from Hakim Sabzevari University, Sabzevar, Iran, in 2017 and 2019, respectively. Her research interests include robotics and machine learning.

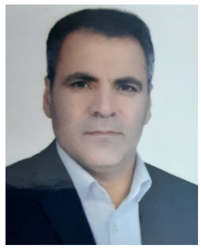

AHMAD HAJIPOUR received the B.Sc. degree in control engineering from the Ferdowsi University of Mashhad, Iran, in 2002, and the M.Sc. and Ph.D. degrees in control engineering from the Shahrood University of Technology, Iran, in 2004 and 2009, respectively. Since 2011, he has been an Associate Professor with the Department of Electrical Engineering, Hakim Sabzevari University. His research interests include fractional calculus, robotics, and machine learning.

HAMIDREZA TAVAKOLI received the B.Sc. degree in electronic engineering from the Ferdowsi University of Mashhad, in 2000, and the M.Sc. and Ph.D. degrees in electronic engineering from the Iran University of Science and Technology, in 2003 and 2014, respectively. Since 2015, he has been an Assistant Professor with the Department of Electrical Engineering, Hakim Sabzevari University. His research interests include robotics, machine learning, and machine vision.

ABBAS NASRABADI received the M.Sc. degree from Semnan University, Iran, in 2008. Since 2010, he has been a Lecturer with the Department of Mechatronic Engineering, Hakim Sabzevari University. His research interests include robotics and machine vision.